Formation mechanism of polycyclic aromatic hydrocarbons in benzene combustion: Quantum chemical molecular dynamics simulations

Biswajit Saha,[1] Stephan Irle,[1,2,a)] and Keiji Morokuma[1,b)]
[1]*Fukui Institute for Fundamental Chemistry, Kyoto University, Kyoto 606-8103, Japan*
[2]*Department of Chemistry and Institute for Advanced Research, Nagoya University, Nagoya 464-8602, Japan*

(Received 16 March 2010; accepted 10 May 2010; published online 8 June 2010)

High temperature quantum chemical molecular dynamics simulations on the polycyclic aromatic hydrocarbon (PAH) formation during combustion of benzene were performed using the density-functional tight-binding (DFTB) method. Systems with varying H/C of 0.8, 0.6, 0.4, and 0.2 and temperatures of T_n=2500 K and T_n=3000 K were employed for the study of the PAH formation and growth mechanism, and trajectories were analyzed by recording average C:H compositions, common elementary reactions and molecular species, ring count, and other characteristic quantities as functions of time. We found that at H/C=0.8 mostly short polyacetylenic hydrocarbons were formed, and no significant PAH growth was found. At lower H/C ratio, longer polyacetylenic chains started to form and new five- and six-membered rings were created due to chain entanglement. Significant PAH growth forming only pericondensed PAHs was observed at lower H/C ratios of 0.4 and 0.2. In addition, smaller hydrocarbon species, such as C_2H_2, C_2H, and C_2, are constantly produced by fragmentation of hydrocarbons (unimolecular reactions) and remain common species, although they are simultaneously consumed by the H-abstraction-C_2H_2-addition growth mechanism. Hydrogen is found to have a clear inhibitive effect on PAH and carbon cluster growth in general, in agreement with recent experimental observations. © *2010 American Institute of Physics*. [doi:10.1063/1.3447895]

I. INTRODUCTION

Understanding the formation mechanism of polycyclic aromatic hydrocarbons (PAHs) is one of the most challenging topics in the area of hydrocarbon fuel combustion and pyrolysis. PAHs are formed during pyrolysis and in the main oxidation zone of the flame and grow to high-molecular-weight species.[1] Interest in the detailed formation mechanism has recently significantly increased due to environmental concerns regarding pollutant emission from combustion devices.[2] Moreover, the formation of PAHs and their hydrogen-deficient precursor molecules is involved in the formation of fullerenes[3–5] and nanotubes[6] in their combustion synthesis and in the chemical evolution of the interstellar medium.[7]

The hydrocarbon flame is a very complicated system due to the many chemical and physical processes simultaneously involved in high temperature reactions. During the combustion, many different carbon-containing molecular and supramolecular species have been identified. Among them are very short-lived species, such as radicals and ions, and very stable compounds such as the water gas compounds CO, CO_2, H_2, and H_2O. In addition, in a fuel-rich flame, PAHs and soot are well known and common products. Experimental techniques such as mass spectroscopy are used to identify the molecular composition of these PAHs, but determination of their molecular structure at combustion temperatures still remains a challenging problem. Mass-spectroscopic experiments on flame ions were performed by Homann group as early as 1987.[8] They recorded the H/C ratio of PAH species from acetylene flames in dependence on the burner distance and postulated that the thermodynamically most stable PAH species with the maximum number of condensed rings C_xH_y represent a "band" of growth that is followed by the recorded species. Based on this observation, it was postulated that the PAH platelets should have little to no pentagons and little hydrogen addition or loss defects.[1] Such a structural proposal for the intermediate species is hard to reconcile with the fact that product species such as fullerene cages and soot particles are generally curved.[4] H/C ratios in PAHs based on *in situ* mass spectroscopy cannot give direct information regarding the carbon skeleton of the high-temperature species, and the structural postulate presented by Homann *et al.* is based solely on thermodynamic reasoning while overlooking the kinetics of structural transformation and annealing processes before the molecular species can be detected in the mass spectrometer. Moreover, the concentration of flame ions was recently found to be lower by factors of 10^4–10^6 than that of neutral PAHs.[9] Therefore, the concentration of hydrocarbon ions is too low to play an important role in flame chemistry, and an investigation of the evolution of ionic species alone cannot be expected to yield a complete understanding of the PAH formation mechanism. Very recently, gas-phase condensation experiments such as laser pyrolysis and laser ablation have been performed by Jäger *et al.*[10] to understand PAH formation using hydrocarbon fuel

a)Electronic mail: sirle@iar.nagoya-u.ac.jp.
b)Electronic mail: morokuma@fukui.kyoto-u.ac.jp.

species such as C_2H_2, C_2H_4, and C_6H_6. They observed that at lower temperature (<1700 K) PAHs consisting of mainly three to five rings are formed, whereas at higher temperature (>3500 K), fullerene or fullerenlike structures were dominantly formed. They also suggested that the formation pathway of the soot particles was characterized by the formation of carbon chains in line with our previous simulations.[11]

Although it is certainly beyond reasonable doubt that PAH molecules grow into soot particles,[12] neither chemical composition of the neutral intermediates, their radical character, nor prevalent routes of condensation mechanisms have been clarified in experimental studies. Therefore, theoretical studies are of viable importance for studies in this field, and the PAH formation mechanism was first studied using transition state theory for selected chemical species that were chosen based on assumptions for the reaction mechanisms.[13,14] As the smallest compound in the PAH series, naphthalene formation was modeled via two routes: at first by the sequential addition of C_2H_2 to a phenyl radical and second by the combination of resonantly stabilized radicals. The first mechanism is usually known as the H-abstraction-C_2H_2-addition (HACA) mechanism and has become somewhat of a consensus in the combustion community.[13] Formation and consumptions of single-ring aromatic hydrocarbons and their precursors in premixed benzene flame were also studied using kinetic modeling.[15] According to these studies, benzene consumption occurs due to H abstraction reactions, and thus the formation of the phenyl radical (C_6H_5) was deemed important. On the condensation side of the mechanisms, growth pathways leading to PAHs containing up to six condensed rings were studied by Richter *et al.*[16] They confirmed in kinetic models that PAH growth can occur following the proposed HACA mechanism, but alternative pathways cannot be excluded by such studies. Yet, when it comes to highly accurate quantum chemical reaction pathway studies, exhaustive theoretical modeling of PAH growth have only reached to the system size of the indene and $C_{10}H_{11}$ molecule.[17,18]

To overcome the computational limitations of detailed tracking of individual reaction pathways, the growth of aromatic hydrocarbon in benzene laminar flame has been modeled using kinetic Monte Carlo and molecular dynamics (MD) methods based on classical potentials adjusted to the results of quantum chemical calculations for small model species.[12] In general, pyrolysis and combustion MD simulations are hampered by the fact that H abstraction reactions are occurring at a very slow rate[19] even for semiclassical reactive force field (ReaxFF) potentials.[20] Moreover, because of the importance of π-conjugation, aromatic Clar sextets, and the stability differences of radical species, fully quantum chemical MD (QM/MD) simulation of the combustion process are clearly preferable over classical force field approaches.

A brute force QM/MD approach considering both fuel and O_2 molecules as reaction system is computationally not feasible even on today's supercomputer systems due to the long time scales involved in H abstraction reactions. Since it is obvious that oxidation will eventually lead to the exothermic products H_2O, CO, and CO_2, which provide the heat of the combustion, the resulting oxygen-containing products are closed-shell molecules with low reactivity and not expected to participate much in the growth process. Hence, in our previous study of fullerene formation in benzene flames[11] as well as in the present work, we modeled the oxidation process by gradually removing hydrogen atoms during constant temperature QM/MD simulations. In the present study, we chose reaction systems initially consisting of 27 benzene molecules and subsequently removed hydrogen atoms during nonequilibrium MD simulations until a desired H/C ratio was achieved, for which we followed chemical transformations for tens of picoseconds. During the QM/MD simulations, we recorded fragment sizes and C:H composition, sp^n hybridization, and the numbers of carbon backbone pentagons/hexagons/heptagons as functions of time.

II. METHODOLOGY

A. Density-functional tight-binding quantum chemical potential

All QM/MD simulations were performed with the density-functional tight-binding (DFTB) method as implemented in the program package developed by Frauenheim, Seifert, Elstner, and co-workers.[21] DFTB is an approximate density functional theory (DFT) method based on the tight binding approach and uses an optimized minimal linear combination of atomic orbitals (LCAO), Slater-type valence-only basis set, in combination with a two-center approximation for the Hamiltonian matrix elements and diatomic repulsive potentials. We have compared its performance with *ab initio* G3-type and first principles B3LYP benchmark data reported by Kislov and Mebel[18] for the prediction of reaction barrier heights, energetics, and molecular geometries of radical PAH formation pathways for systems with up to ten carbon atoms.[11] We compared energetics predicted by both non-charge-consistent (NCC) and self-consistent-charge (SCC) incarnations of DFTB after reoptimization of the structures at the respective level.[11] We noted that the NCC-DFTB and SCC-DFTB energies and, consequently, relative energies and barrier heights are rather close since the charge polarization in these systems is generally small. The agreement of DFTB energetics with that of the computationally far more expensive B3LYP and G3(MP2/CC) data was remarkable. Following our previous work,[11] we chose to apply a finite Fermi–Dirac electronic temperature T_e of 5000 K to ensure roughly equal population of the radical's singly occupied molecular orbitals, which is crucial for NCC-DFTB-based QM/MD simulations. A detailed discussion on the formalism and use of finite electronic temperature within DFTB is given elsewhere.[22] Our benchmark studies justify the use of the computationally inexpensive NCC-DFTB level of theory in combination with electronic temperature for the quantum chemical potential underlying MD simulations of benzene combustion and confer a near-DFT accuracy on such simulations. In the remainder of this article we will use the term "DFTB" in place of "NCC-DFTB" for simplicity.

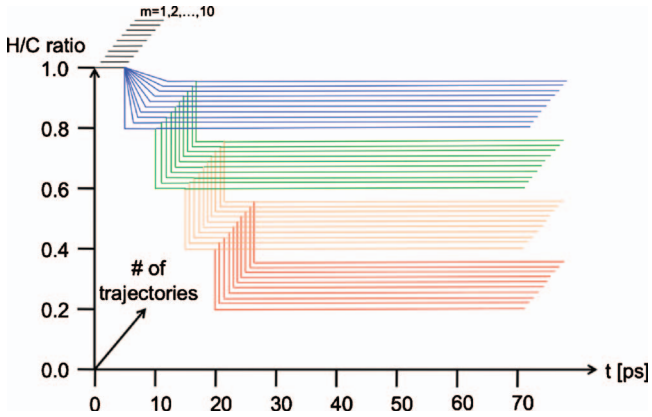

SCHEME 1. Hydrogen removal scheme during simulations to achieve the described H/C ratio.

B. Molecular dynamics

To ensure constant density, the simulations were carried out using periodic boundary conditions (PBCs). The gamma-point approximation was used for the PBC cell image interaction calculations. All trajectories were computed by calculating analytical DFTB energy gradients on the fly with a Verlet integrator using 0.48 fs as time integration interval Δt. We have checked in microcanonical MD simulations that this choice for Δt is small enough to ensure proper time integration for the higher frequency C–H stretch vibrations at the given system temperature. Two target nuclear temperatures, $T_n=2500$ K and $T_n=3000$ K, were maintained using scaling of atomic velocities; the scaling was performed regularly after every 4.84 fs, and additionally scaling occurred at any given time step with a random probability of 10%, thereby an overall scaling probability of 20% was applied. We computed a total of 20 trajectories (10 trajectories for each temperature) for each target system's H/C ratio. MACMOLPLT (Ref. 23) was used for graphical visualization of the trajectories.

C. Modeling gas-phase benzene oxidation

The starting model system consisted of 27 benzene molecules stacked in three layers of nine molecules arranged in a three by three quadratic plane with an interlayer distance of 5.5 Å and closest intermolecular H contacts of 2.8 Å, in a cubic cell with 30 Å side length. The particular arrangement of the benzene molecules is not crucial as the layered structure very quickly disappears at the high system temperatures. The initial density of the model system is 0.130 gm/cm^3, which is high for gaseous benzene but low when compared to the density of liquid benzene density, which is 0.87 gm/cm^3. We have used such a high pressure/density environment to accelerate the initial PAH growth. The carbon density of the model system is 0.120 gm/cm^3.

As already mentioned, we do not include oxygen molecules in our model systems; instead, we remove 30 randomly selected hydrogen atoms from the system every 5.00 ps until a desired H/C ratio was achieved. As illustrated in Scheme 1, we begin with ten trajectories for each target temperature starting from the initial geometry, generated by ten different sets of random initial velocities to the atoms. For 5.00 ps, no H atoms were removed. These initial trajectories are named $m=1,2,3,\ldots,10$. These trajectories were analyzed in Sec. III for the dynamics for $t<5$ ps. As illustrated in Scheme 1, using the final geometries and velocities of the $m=1$ trajectory and by removing ten different sets of randomly selected 32 hydrogen atoms, we created ten new trajectories at each temperature with the first target system H/C ratio of $130/162=0.802$ (we denote them as $H/C=0.8$). These $H/C=0.8$ trajectories were then continued up to a total simulation time of 70.06 ps. After 5.00 ps into each $H/C=0.8$ trajectory, we spawn a new trajectory by randomly removing more 33 H atoms to generate a trajectory having the lower H/C ratio of $97/162=0.599$ (in short $H/C=0.6$), and these trajectories are also continued up to a total simulation time of 70.06 ps. The same procedure was applied, as shown in Scheme 1, to spawn ten $H/C=65/162=0.401$ (in short $H/C=0.4$) trajectories and then $H/C=32/162=0.198$ (in short $H/C=0.2$) trajectories. We named the ten trajectories for each T_n and H/C ratio P2500Kx_n and P3000Kx_n, where $n=1-10$; $x=8$, 6, 4, and 2 correspond to H/C ratios of 0.8, 0.6, 0.4, and 0.2, respectively. The target H/C ratios of 0.8, 0.6, 0.4, and 0.2 have corresponding densities of 0.128, 0.126, 0.124, and 0.122 gm/cm^3, respectively. Thus, a total of 40 trajectories for each temperature was generated, which share the previous parts of the trajectories run during the stepwise 5.00 ps H removal stages (see Scheme 1 for an explanation of the generation of the trajectories). Benzene oxidation is thus simulated by hydrogen removal instead of allowing chemical reactions of O_2 molecules with the hydrocarbons that would eventually lead to exothermic products H_2O, CO, and CO_2 via the more reactive radical species OOH and OH. We have discussed the merits and disadvantages of such a simplified approach in our previous work, and we only wish to refer here to the detailed discussion given in Ref. 11. Since it is not feasible to perform more "realistic" simulations on present-day computers even with the relatively inexpensive DFTB potential, we refrain from detailed analysis regarding all possible reaction pathways occurring in our simulations, and instead focus more on the qualitative aspects of cluster growth such as fragment size, H/C ratio, carbon sp^2 versus sp hybridization, and ring count statistics as a function of simulation time.

III. RESULTS AND DISCUSSIONS

A. Initial reactions (t=0–5 ps, H/C=1)

For both target temperatures, we have computed ten different trajectories with all atoms in the model system for the first 5.00 ps. During this initial 5.00 ps time interval, where all 162 hydrogen atoms were present in the system, we already observed various radical reactions due to thermal decomposition and the high benzene density, in particular, for the case of $T_n=3000$ K. The hydrocarbon species different from benzene, resulting from reactions occurring at $T_n=2500$ K, are products of hydrogen abstractions with $2C_6H_7$, $3C_6H_5$, C_6H_4, 3H(m=1), $2C_6H_5$, 2H(m=2), C_6H_8, $3C_6H_7$, $3C_6H_5$, $2C_4H_3$, C_2H, C_2, 3H(m=3), C_6H_7, $2C_6H_5$, H(4), C_6H_7, $4C_6H_5$, 3H(m=5), $C_{12}H_{11}$, C_6H_8, C_6H_7, $5C_6H_5$, 3H(m=6), $4C_6H_5$, C_4H_5, C_2H, 4H(m=7), $2C_6H_5$, 2H(m

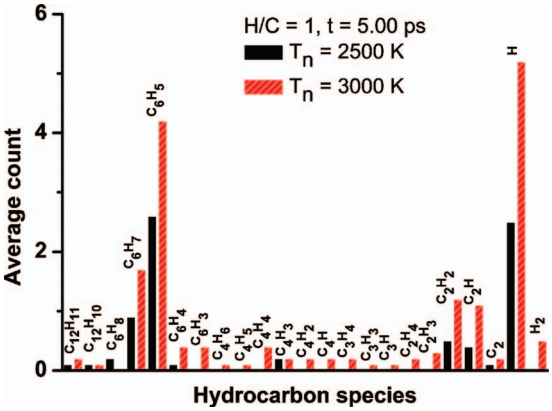

FIG. 1. Average number of C:H composition of species created with H/C=1 and time t=5.00 ps. For details, see text.

=8), C_6H_7, C_6H_5, $4C_2H_2$, $2C_2H$, H(m=9), $C_{12}H_{10}$, C_4H, C_2H_2, and 5H(m=10); clearly, the carbon framework of the benzene molecules remains unmodified in 5(m=1,2,4,5,8) cases, whereas in other cases biphenyl-like structures are formed and/or small fragments have created due to thermal decomposition. The nonbenzene species created for T_n=3000 K are more prominent and involved modifications of the carbon frameworks: $2C_6H_7$, $7C_6H_5$, $2C_4H_4$, C_4H, C_2H_3, $4C_2H_2$, C_2, H_2, 7H(m=1), C_6H_7, $5C_6H_5$, 4H(m=2), $C_{12}H_{11}$, $4C_6H_7$, $4C_6H_5$, C_6H_3, C_4H_2, C_2H_3, C_2H_4, $2C_2H_2$, 5H(m=3), $C_{12}H_{10}$, C_6H_7, $6C_6H_5$, C_4H_5, C_2H_2, 6H(m=4), $4C_6H_7$, $4C_6H_5$, C_6H_4, C_4H_4, C_4H_3, C_2H_2, C_2H, 4H(m=5), C_6H_7, $4C_6H_5$, C_6H_4, C_4H_6, C_4H_4, $5C_2H$, H_2, 6H(m=6), $C_{12}H_{11}$, $2C_6H_7$, $5C_6H_5$, C_6H_4, C_4H_3, C_3H_4, C_3H_3, $3C_2H_2$, C_2H, H_2, 5H(m=7), $2C_6H_7$, $5C_6H_5$, C_4H, C_2H_4, C_2H_2, C_2H, C_2, H_2, 5H(m=8), $3C_6H_7$, $3C_6H_3$, C_3H_4, C_2H_3, C_3H, $2C_2H$, H_2, 6H(m=9), $3C_6H_7$, $4C_6H_5$, C_4H_2, C_2H, and 4H(m=10). It was observed that in some cases at T_n=3000 K, H_2 molecules formed due to the high abundance of H radical. The average C:H composition (averaged over ten trajectories) of different species (excluding C_6H_6 species) present at the end of the 5 ps simulations at the two temperatures are displayed in Fig. 1, which shows a pronounced temperature effect since at higher temperature a greater variety of hydrocarbon species was created. Under these circumstances, the initial 5.00 ps cannot be considered an equilibration period, but rather represents benzene pyrolysis exhibiting initial reactions preceding our programed hydrogen removal simulations. The initial reactions are typically hydrogen abstractions, creating phenyl and H atom radical species: $C_6H_6 \rightarrow C_6H_5+H$. Follow-up reactions of this abstraction become generally much faster once the phenyl and H radical species are created. In particular, the H radical is sometimes found to react with abundant benzene to create the cyclohexadienyl (C_6H_7) radical. At T_n=3000 K, further decomposition reactions such as $C_6H_5 \rightarrow C_6H_4+H$ and $C_6H_6 \rightarrow C_4H_4+C_2H_2$ or $C_2H_3 \rightarrow C_2H+H_2$ are also observed. No five-membered C_5H_y ring species are observed during this initial reaction period. In reference to experimental findings, we note that small hydrocarbon species such as C_2H, C_2H_3, C_2H_5, C_3H, C_3H_3, C_3H_5, C_4H, C_4H_3, C_4H_5,

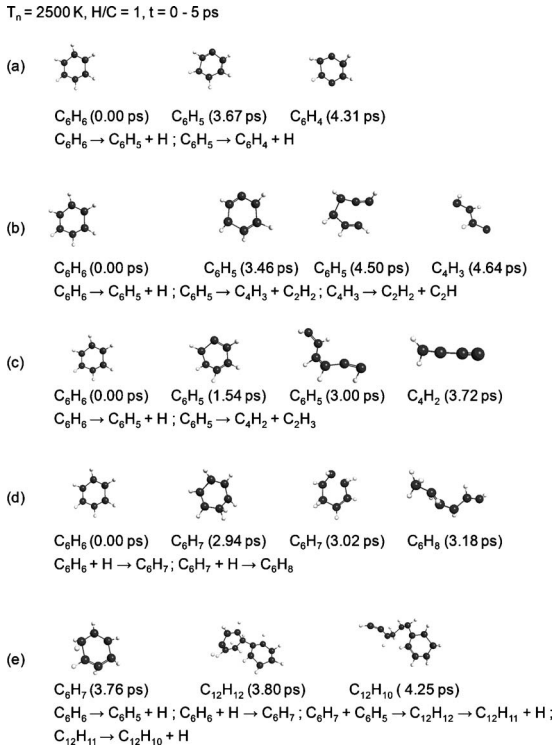

FIG. 2. Snapshot geometries of initial reactions at T_n=2500 K with H/C=1 during t=0–5 ps.

C_4H_7, C_5H_3, C_5H_5, and C_6H_5 were also observed in premixed benzene/oxygen/argon flames under synchrotron photoionization.[24]

Some of the typical reactions and associated molecular structures observed during the first 5 ps of simulations with H/C=1 are displayed in Figs. 2 and 3 for T_n=2500 K and T_n=3000 K, respectively. At T_n=2500 K, mostly benzene molecules (C_6H_6) undergo thermal decomposition and form C_6H_5 radicals ($C_6H_6 \rightarrow C_6H_5+H$) and the created H reacts with the C_6H_6 to form C_6H_7 ($C_6H_6+H \rightarrow C_6H_7$). In some cases, the C_6H_5 radicals were observed to undergo further decomposition to C_6H_4. Figure 2(a) shows the formation of a *para*-C_6H_4 species. Figure 2(b) shows a C_6H_5 unit undergoing ring opening and subsequently forming smaller hydrocarbons ($C_6H_5 \rightarrow CHCHCHC+C_2H_2$). CHCHCHC exhibits further decomposition to form C_2H_2 and C_2H species ($CHCHCHC \rightarrow C_2H_2+C_2H$). Thus, smaller, entropically favored and reactive hydrocarbon species such as C_2H_2 and C_2H are formed as a result of high-temperature unimolecular decomposition. Figures 2(c) and 2(d) show two more examples where benzene undergoes thermal decomposition, forming smaller hydrocarbons CH_2CCC and $CH_3CHCHCHCHCH$. Figure 2(e) shows an example where C_6H_7 and C_6H_5 bind to form $C_6H_7-C_6H_5$, which subsequently undergoes H abstractions to form the thermodynamically more stable $C_{12}H_{10}$ species ($C_6H_6 \rightarrow C_6H_5+H$; $C_6H_6+H \rightarrow C_6H_7$; $C_6H_7+C_6H_5 \rightarrow C_6H_6-C_6H_6 \rightarrow C_6H_6-C_6H_5+H$; and $C_6H_6-C_6H_5 \rightarrow C_6H_5C_6CHCHCHCHCCH+H$). At higher temperature T_n=3000 K, it was found that the system becomes more reactive and much more smaller hydrocarbon species were created, as evident in Fig. 1. Figures 3(a)–3(c) display selected fragmentations (unimolecular reactions) at

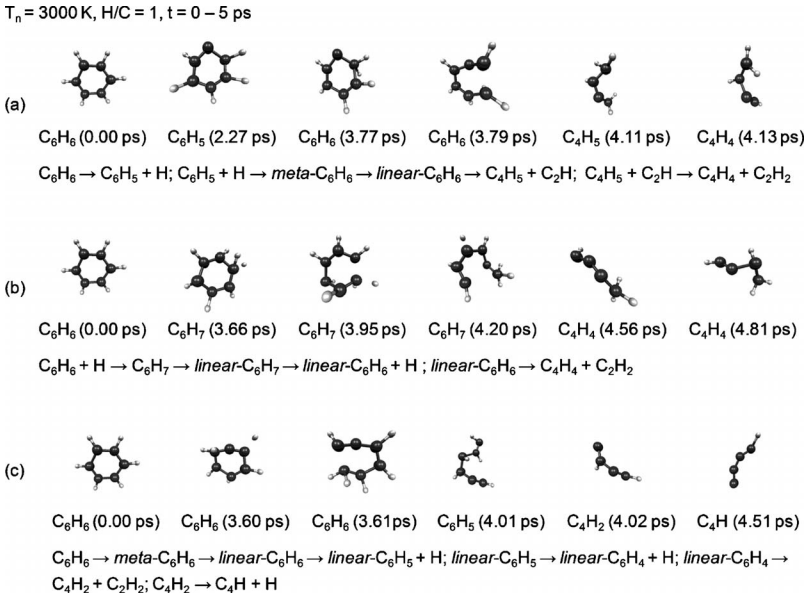

FIG. 3. Snapshot geometries of the initial reactions at T_n=3000 K with H/C=1 during t=0–5 ps.

the higher temperature, where smaller species such as CH_2CHCCH and C_4H were created. In this case, ring opening occurred either via C_6H_5 radical or C_6H_7 formation, and fragmentations were observed after the formation of linear hydrocarbon species.

B. Cluster growth and ring formations: Effect of H/C ratio and temperature

As discussed above and shown in Scheme 1, we created initial conditions for H/C=0.8, 0.6, 0.4, and 0.2 by randomly removing H atoms from trajectories with higher H/C ratio. Although all trajectories share the m=1 initial trajectory as described above, we expect similar behavior if any of the m=2,3,...,10 initial trajectories had been chosen instead. The arbitrary removal of hydrogen atoms from the system obviously created many more radical species, in addition to those formed due to the preceding thermal decomposition of the H/C=1 system; consequently, the system became more reactive and larger hydrocarbon species started to form. Some of the representative reactions occurring at this stage are displayed in Fig. 4 for various H/C ratios. Figure 4(a) shows that C_6H_7 added to C_6H_4 to form a biphenyl-like structure ($C_6H_7+C_6H_4 \rightarrow C_{12}H_{11}$). Subsequently, $C_{12}H_{11}$ caught H and formed the less stable $C_{12}H_{12}$ species, which experienced isomerization with the resulting opening of one of the two six-membered rings, that re-emerged as a five-membered ring plus one CH_3 group attached. At the end of a total simulation time of 10 ps, found in some cases species such as $C_{12}H_{11}$ consisting of one five-membered ring and one six-membered ring are formed. Figures 4(b)–4(d) show examples where C_6H_6 underwent ring opening by loosing H, subsequently reacting with other linear species to form $C_{12}H_6$ (b), C_6H_5CCCC (c), and C_6H_5CC (d) hydrocarbons. Figures 4(c) and 4(d) show hydrocarbon growth due to the

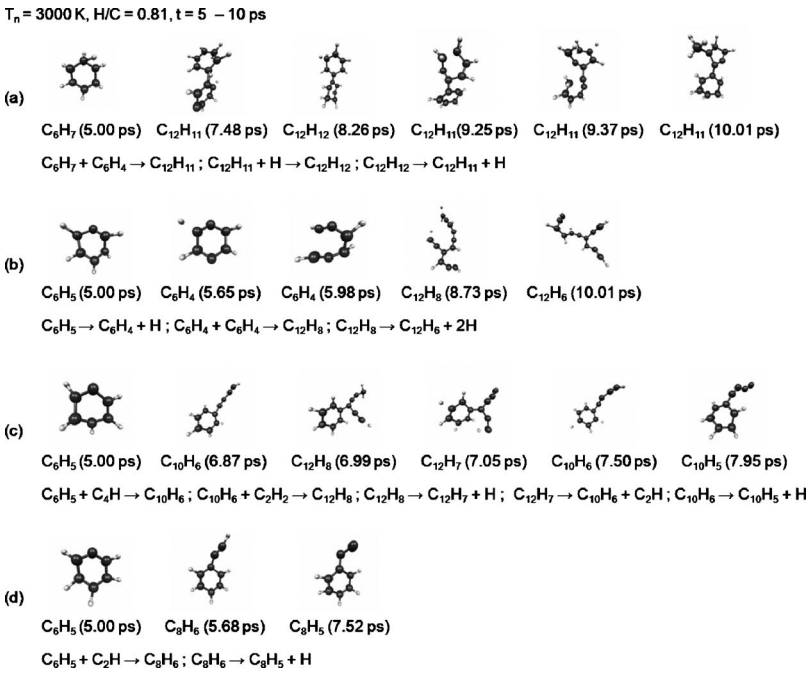

FIG. 4. Snapshot geometries of the initial reactions at T_n=3000 K with H/C=0.81 during t=5–10 ps.

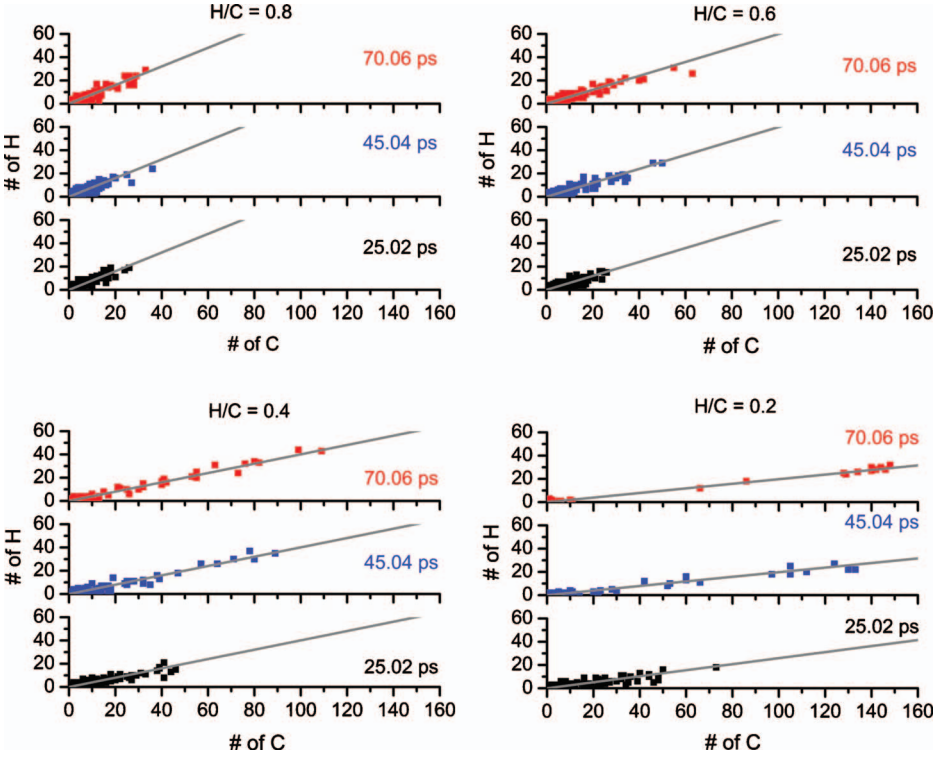

FIG. 5. Hydrocarbon formation and growth with time for T_n=2500 K. Each point corresponds to a species of the form C_xH_y. The (gray) line corresponds to the H/C ratio of over all system. Data points plotted for ten simulations.

addition of C_2H_2- or C_2H-like species. After this point, the number of reactions became too large to identify major reaction pathways, but we will discuss general observations in the remainder of this section.

The C:H compositions of hydrocarbons formed during simulations are shown in Figs. 5 and 6 as a function of time for H/C=0.8, 0.6, 0.4, and 0.2. Data points are plotted for as averages over ten trajectories for each temperatures of T_n=2500 K and T_n=3000 K. Each data point on the graph corresponds to a hydrocarbon of the form C_xH_y. In order to

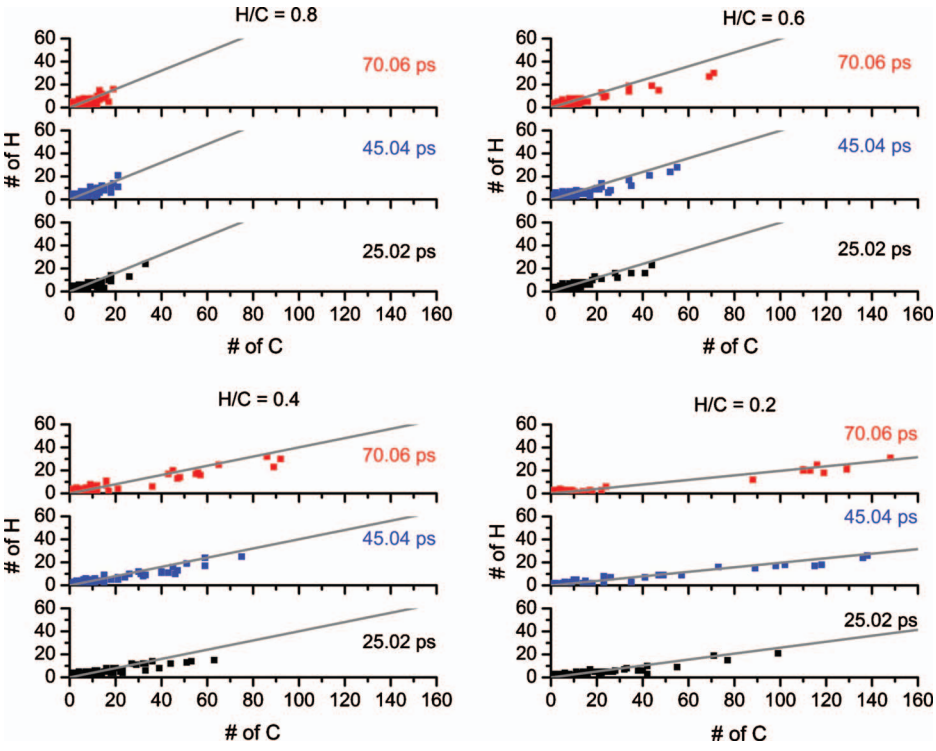

FIG. 6. Hydrocarbon formation and growth with time for T_n=3000 K. Each point corresponds to a species of the form C_xH_y. The (gray) line corresponds to the H/C ratio of over all system. Data points plotted for ten simulations.

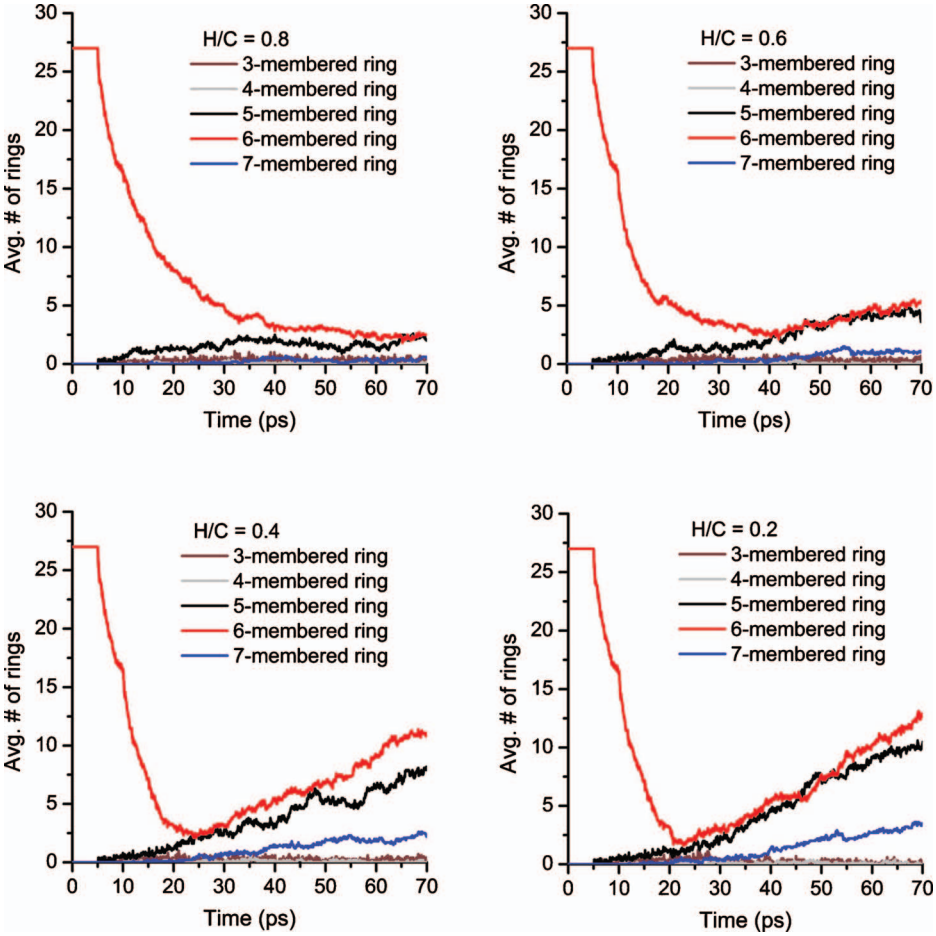

FIG. 7. Formation statistics of three- to seven-membered rings as a function of time for T_n=2500 K. Averaged over ten simulations (t=5–70.00 ps).

determine the stoichiometry of hydrocarbon species created in the trajectories (in other words, the C:H composition), we used cutoff radii of 1.90, 1.70, and 1.50 Å for C–C, C–H, and H–H bond lengths, respectively. These cutoff radii are the result of extensive numerical tests regarding the long-term stability of covalent bonds in the present hot, vibrationally excited systems. The continuous line corresponds to the overall H/C ratio of the system. It is apparent from this figure that for H/C=0.8 and 0.6, the largest hydrocarbons of the form $C_{30}H_{20}$ and $C_{40}H_{20}$, respectively, are formed at the end of the simulations, in addition to many hydrocarbon species of size $\sim C_{15}H_{10}$, while smaller species are also present. For H/C=0.2, the largest hydrocarbon species corresponds to $C_{150}H_{20}$, with only a few other smaller hydrocarbons being present. Thus, we find that at the end of the simulations a large carbon cluster with small number of hydrogen is formed, which contains almost all of the atoms present in the system. On the other hand, for H/C=0.4, big molecular clusters are distributed over the entire size rage ($\sim C_{20}H_7-C_{100}H_{40}$). This implies that at the H/C ratio of 0.4, two or three big clusters can form but do not merge to become a single monolithic cluster. This fact implies that the presence of H slows down the growth processes.

The averages of the number of different size rings formed during the course of the simulations is displayed in Figs. 7 and 8 for T_n=2500 K and T_n=3000 K, respectively. These figures exhibit a very interesting dependence of the ring opening and formation processes on the system H/C ratio and temperature. The number of six-membered rings drops very fast (e.g., H/C=0.8, up to ~40 ps) or even more sharply (e.g., H/C=0.2, up to ~20 ps) as H is removed from the system, and the number of six-membered rings present in the system around this stage is only 1 or 2 for T_n=2500 K (see Fig. 7). The ring opening is much more rapid at T_n=3000 K (see Fig. 8). This implies that the ring opening process and, hence, the creation of polyacetylene-like structures and/or small hydrocarbon chains is much faster compared to the ring formation during this stage. For T_n=2500 K, at higher H/C ratio the number of five-, six-, and seven-membered ring is very small, say, for H/C=0.8 and 0.6 these are 1, 2, and 0, respectively, at ~40 ps. The number of rings does not increase much at these high H/C ratios. On continuation of the simulations up to 70 ps, these numbers become 2, 2, and 0 (for H/C=0.8) and 5, 5, and 1 (H/C=0.6), respectively. Thus, we find that a higher H/C ratio slows down the ring formation/growth processes. On the other hand, the corresponding numbers for H/C=0.4 are 2, 2, and 0, and 2, 1, and 0 for H/C=0.2 at ~20 ps (see Fig. 6). However, after 70 ps of simulations, these numbers increase at a fast rate. The numbers of five-, six-, and seven-membered rings formed at that stage are 6, 11, and 2 (H/C=0.4) and 10, 12, and 2 (H/C=0.2) (see Fig. 7). The general trend of a much faster reaction and/or ring formation

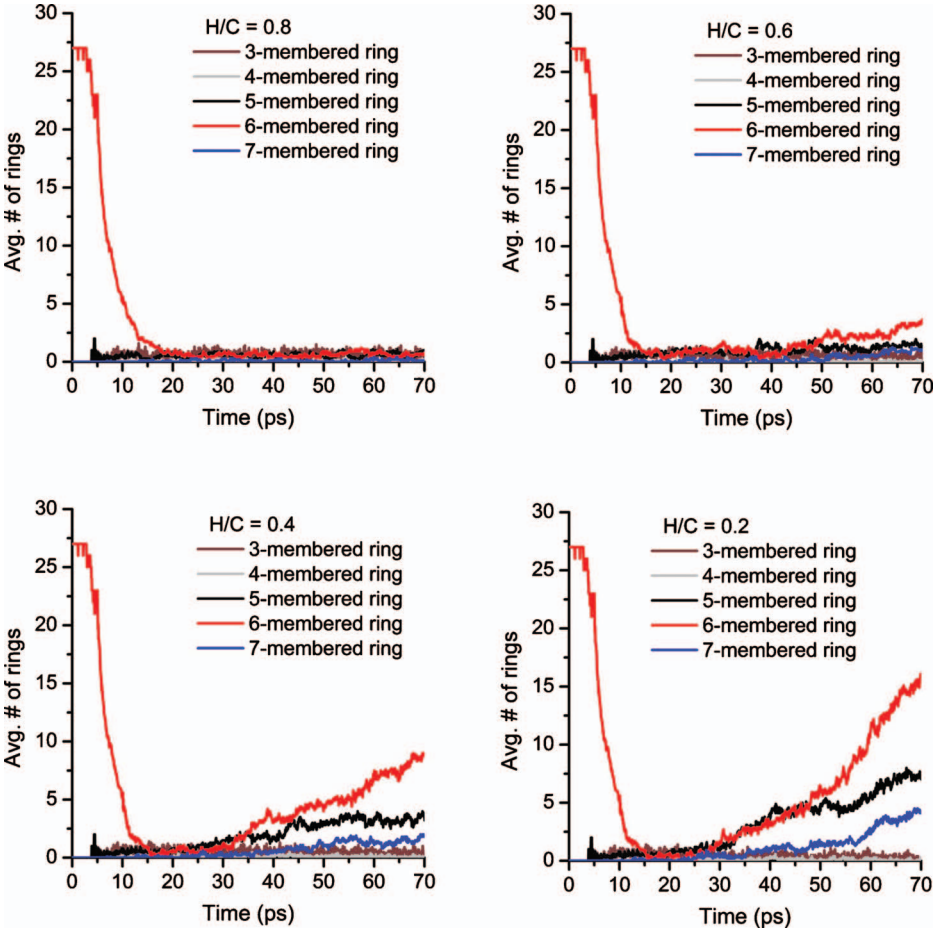

FIG. 8. Formation statistics of three- to seven-membered rings as a function of time for T_n=3000 K. Averaged over ten simulations (t=5–70.00 ps).

at higher temperature of T_n=3000 K is observed clearly from Fig. 8. Almost all benzene rings had been broken around 15 ps irrespective of the system's H/C ratio. No significant ring formation occurred even after 70 ps of simulations for H/C=0.8. For H/C=0.6, at the end of the simulations, only one five-membered ring, three six-membered rings, and one seven-membered ring formed/present. On the other hand, for lower H/C ratios, significant ring formation and growth are observed. At the end of the simulations, 3 five-membered rings, 8 six-membered rings, and 1 seven-membered ring for H/C=0.4 and 6 five-membered rings, 16 six-membered rings, and 7 seven-membered rings for H/C=0.2 were formed. For H/C=0.2 at both temperatures, we observe a clear trend toward further ring formation. Besides these small-size rings, in some species larger rings such as eight-, nine-, and ten-membered rings or even larger macrocycles developed. Continued annealing at high temperature transform these larger rings into more stable smaller ones, around the five- or six-membered ring size. Thus, we find that lower H/C ratios and higher temperature promote ring formation. One interesting feature revealed from these simulations that the formation of higher-membered rings (macrocycle) may occur when sufficiently large polyyne chains are present in the system.

As an overall trend, we note that in the trajectories with a given H/C system ratio, larger clusters tend to have only slightly lower H/C ratios than the system value, while smaller fragments have correspondingly slightly higher H/C ratios. Most importantly, as long as hydrogen is present in the system *we do not find a preference in growth toward maximally conjugated PAHs* that have significantly lower H/C ratios than the overall system's H/C ratio. The average curvature values of these structures, formed at 70.06 ps with H/C=0.2, are significant with ~0.17 $Å^{-1}$ but somewhat lower than the curvature values ~0.20 $Å^{-1}$ we obtained during self-assembly of giant fullerenes[11,25] (see Table SI in the supplemental information[26]) from pure C_2 feedstock without any hydrogen present. In the presence of hydrogen, somewhat more planar structures seem to be formed preferentially. The reason for this is discussed further below.

We noticed that among several small hydrocarbon species, C_2, C_2H, C_2H_2, and C_2H_3 are formed frequently (see Figs. S2 and S3 in the supplemental information[26]) and are always present in the system during the entire simulation time. Other small species such as C_2H_4, C_3H_3, C_4, C_4H, C_4H_2, and C_4H_4 are also formed in a smaller amount, in dependence on the overall system H/C ratio. Strikingly, and in agreement with the HACA reaction mechanism, C_2 and C_2H are the most abundant species for all H/C ratios. At higher H/C ratios, H/C=0.8 and 0.6, the creation of C_2H_2 species is very prominent and the number of C_2H_2 decreases as the H/C ratio decreases. On the average, $12C_2H$, $10C_2H_2$, and $3C_2$ are present in the system from 40 ps onward, for H/C=0.8. This indicates that PAH growth by the addition of

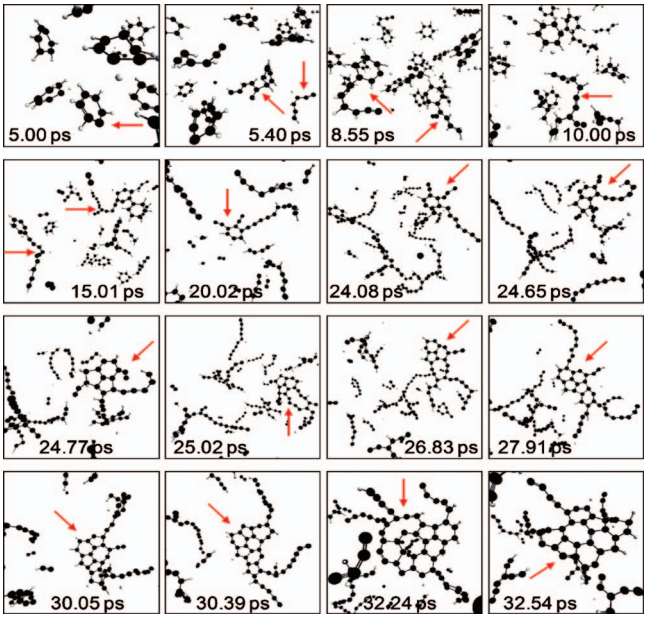

FIG. 9. Snapshots of PAH formation and growth mechanism with T_n=2500 K (P2500K2_10). Arrows denote region where the mentioned event is observed. Carbon and hydrogen atoms are represented by black and gray spheres, respectively. Details are given in text.

C_2H- and C_2H_2-like species at fuel reach condition is more likely. For H/C=0.2, almost no C_2H_2 species remain from 25 ps onward, although several C_2H and C_2 molecules are present in the system. We predict therefore that under strongly oxidizing conditions, the presence of C_2H_2 should be less likely.

C. PAH formation mechanism from QM/MD simulations

Formation and growth mechanism of a PAH are shown using selected snapshots from a representative trajectory (P2500K2_10) with H/C=0.2 in Fig. 9. We observe that the created radical species (either due to thermal decomposition or due the programed H removal) with ring structure easily forms polyacetylene-like structures (5.00, 5.40, 8.55, and 10.00 ps). These polyacetylene-like structures may grow further by reacting with other polyacetylene-like structures, radical species, or benzene molecules present in the system (15.01, 20.02, and 24.08 ps). Usually most of the rings open to form polyacetylene-like structures, and only very few ring could survive (20.02 and 24.08 ps). Thus, these polyacetylene-like structures assemble themselves to form larger and branched polyacetylene-like structures (24.08 ps). Therefore, in some cases, an original six-membered ring can be attached to a polyacetylene-like structure. In the situation where there is no original six-membered ring, the polyacetylene-like structures can catch each other to form new ring five-, six-, or seven-membered rings (24.65 ps). Once a ring (usually five- or six-membered) is formed, the further ring condensation proceeds quite fast (24.65, 24.77, 25.02, 26.33, 27.91, 30.05, 30.39, 32.24, and 32.54 ps). The formation of the first aromatic ring is a crucial event in the formation process of PAH and soot in flame (see also Ref. 27). The snapshot shown at 32.54 ps consists of two five-membered rings, five six-membered rings, and one seven-membered ring and polyacetylyne-like structures attached with this. These polyacetylene-like structures (may) help further ring condensation and growth processes. Thus, a preformed PAH may catch a polyacetylene-like structure at high temperatures. The abovementioned stages are presented in Scheme 2 for both temperatures. As shown in Scheme 2, in the first stage C_6H_n ($n<6$) radical species are created and subsequently polyacetylenic chains form. In the next stage, these linear chains occasionally react to form branched

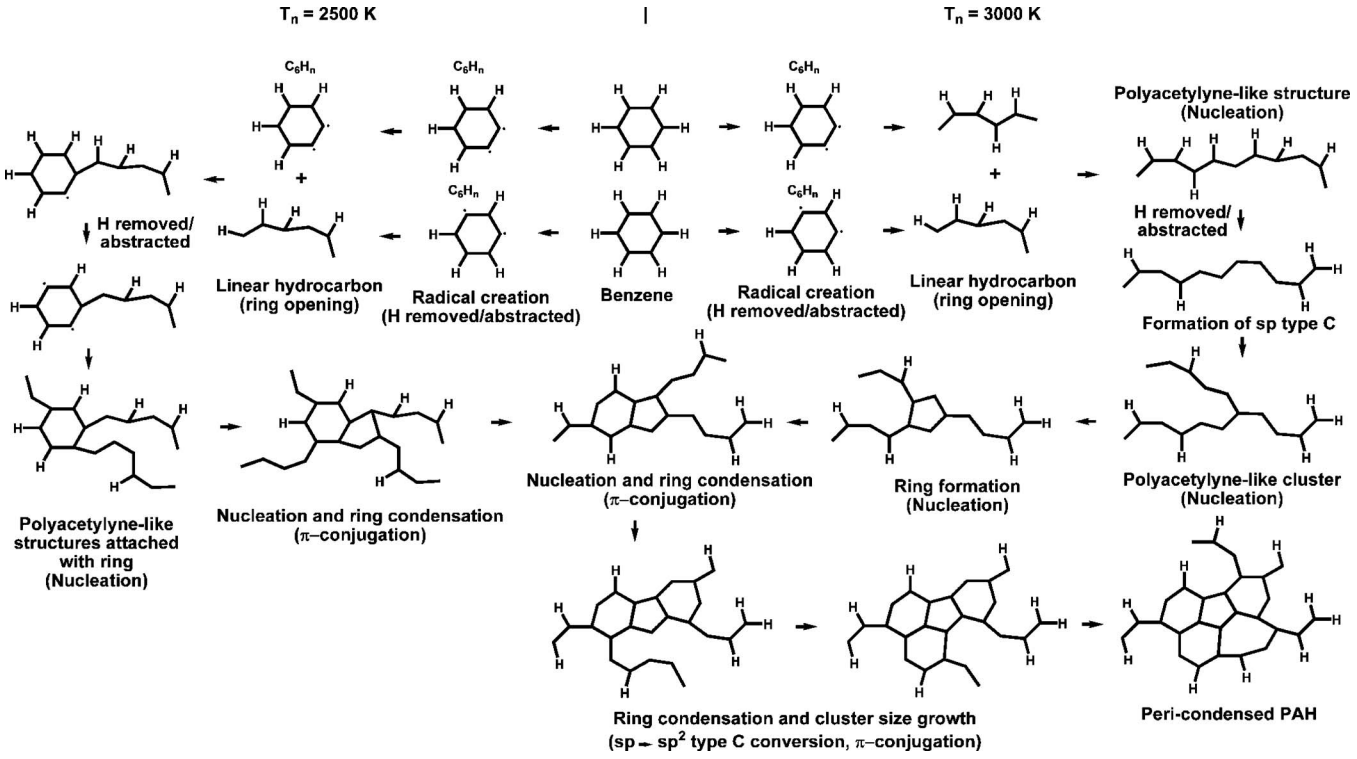

SCHEME 2. PAH formation and growth mechanism.

polyacetylene-like structures, typically initiated by radical centers present somewhere on the chain of carbon atoms. In the third stage these branched polyacetylene-like structures form new five-, six-, and seven-membered or larger rings due to ring condensation, depending on the availability of the free valences. In the fourth stage, further ring condensation growth occurs around this newly formed condensed ring system to form pericondensed rings, and the size of the π-system increases, while sp-type carbon converts to sp^2-type. At higher temperature, we notice a preference for hexagon creation over pentagons, resulting from annealing transformations that occur simultaneously with ring condensation.

In previous carbon-only QM/MD simulations starting from ensembles of C_2 molecules at 2000 K environmental temperature,[25] we had found instantaneous polyyne chain formation and chain entanglement initiating sp to sp^2 transformations. A small pentagon/hexagon/heptagon-containing sp^2-nucleus cluster would grow by rapid ring condensation of the remaining attached polyyne chains, which, in turn, grew by the addition of C_2 units from the outer environment. If a significant curvature is present in the nucleus for a longer amount of time, it becomes kinetically stabilized by the topology of the growing carbon network on its outer rim. Such a basketlike nucleus with polyynes attached resembles an octopus sitting on a rock with arms stretched out radially, and we therefore call these important species "octopus on the rock" structures. In the present PAH simulations, we do not find such species because the ring condensation growth occurs slower due to the presence of hydrogen along the carbon chains. The growing clusters therefore show more moderate curvature as opposed to all-carbon systems.

IV. CONCLUSIONS

MD simulations were performed using DFTB method to study the PAH formation and growth mechanism during benzene combustion at high temperatures. The oxidation of benzene molecules was modeled by removing 30 randomly selected hydrogen atoms every 5.00 ps until the desired H/C ratios were reached, and the systems were then allowed to propagate up to a total simulation time of 70.06 ps. The effects of H/C ratio by considering $H/C=0.8$, 0.6, 0.4, and 0.2 and temperatures using $T_n=2500$ K and $T_n=3000$ K on the formation and growth mechanism were analyzed by recording average C:H compositions, most common elementary reactions and molecular species, ring count, and other quantities as a function of time. We found no significant PAH growth at an H/C ratio of 0.8. At this ratio, only linear small hydrocarbons were formed at $T_n=3000$ K, although small PAH with two or three rings are present for $T_n=2500$ K. Hydrogen is found to have a clear inhibitive effect on PAH and carbon cluster growth in general, in agreement with recent experimental observations.[5] Faster growth occurs at lower H/C ratios. At the end of the simulations, larger PAH with fused five-/six-/seven-membered rings were formed, with polyacetylyne-like structures attached. In agreement with the HACA reaction mechanism, C_2 and C_2H are the most abundant species for all H/C ratios; however, this is not the only route for PAH growth. Other more complex reaction mechanisms were found to contribute to the growth process.

A significant amount of sp-hybridized polyyne-like carbon species remains present up until all hydrogen atoms are removed. The C:H composition of the growing PAH radical species from polyacetylene-like open-chain radical species differs rather little from the H/C ratio of the system, and no tendency toward formation of maximally condensed PAH systems was observed. This finding stands in remarkable contrast to the hypothesis of ordered PAH growth following thermodynamically most favorable species and emphasizes the necessity to consider growth mechanisms that involve open-chain and pentagon-containing intermediate species. It can be expected that upon continuation of the presented simulations for longer time with same H/C ratio, the cluster will not grow significantly since the largest cluster has already consumed nearly all available carbon atoms. Continuation of the simulations for longer time should also lead to further ring condensation processes, as evident from the steep slopes for the number of five- and six-membered rings as shown in Figs. 7 and 8, specifically for $H/C=0.4$ and 0.2. To study the equilibrium composition at a given H/C system ratio, we are currently performing longer simulations with more benzene molecules.

ACKNOWLEDGMENTS

B.S. acknowledges the Fukui Institute for Fundamental Chemistry for Fukui Institute Fellowship and S.I. acknowledges support from the Program for Improvement of Research Environment for Young Researchers from Special Coordination Funds for Promoting Science and Technology (SCF) commissioned by the Ministry of Education, Culture, Sports, Science and Technology (MEXT) of Japan. This work was in part supported by a CREST (Core Research for Evolutional Science and Technology) grant in the Area of High Performance Computing for Multiscale and Multiphysics Phenomena from the Japan Science and Technology Agency (JST). Computer resources made available at the Academic Center for Computing and Media Studies (ACCMS) at Kyoto University as well as at the Research Center for Computational Science (RCCS) at the Institute for Molecular Science (IMS) are acknowledged.

[1] K. H. Homann, Angew. Chem., Int. Ed. **37**, 2435 (1998).
[2] J. O. Allen, N. M. Dookeran, K. A. Smith, A. F. Sarofim, K. Taghizadeh, and A. L. Lafleur, Environ. Sci. Technol. **30**, 1023 (1996); M. F. Denissenko, A. Pao, M. S. Tang, and G. P. Pfeifer, Science **274**, 430 (1996); J. L. Durant, W. F. Busby, A. L. Lafleur, B. W. Penman, and C. L. Crespi, Mutat Res. **371**, 123 (1996); M. Z. Jacobson, Nature (London) **409**, 695 (2001); H. R. Zhang, E. G. Eddings, and A. F. Sarofim, Environ. Sci. Technol. **42**, 5615 (2008).
[3] P. Hebgen, A. Goel, J. B. Howard, L. C. Rainey, and J. B. V. Sande, Proc. Combust. Inst. **28**, 1397 (2000).
[4] A. Goel, P. Hebgen, J. B. V. Sande, and J. B. Howard, Carbon **40**, 177 (2002).
[5] H. Takehara, M. Fujiwara, M. Arikawa, M. D. Diener, and J. M. Alford, Carbon **43**, 311 (2005).
[6] J. Z. Wen, H. Richter, W. H. Green, J. B. Howard, M. Treska, P. M. Jardim, and J. B. Vander Sande, J. Mater. Chem. **18**, 1561 (2008).
[7] D. C. Lis, presented at the 231st Symposium of the International Astronomical Union, Pacific Grove, CA, 2005.
[8] P. Gerhardt, S. Loffler, and K. Homann, Chem. Phys. Lett. **137**, 306 (1987).

[9] Th. Baum, "Positive ionen in 1,3-butadien-niedeedruckflammen," Ph. D. thesis, TU Darmstadt, 1996.
[10] C. Jäger, F. Huisken, H. Mutschke, I. L. Jansa, and T. Henning, Astrophys. J. **696**, 706 (2009).
[11] B. Saha, S. Shindo, S. Irle, and K. Morokuma, ACS Nano **3**, 2241 (2009).
[12] A. Violi and A. Venkatnathan, J. Chem. Phys. **125**, 054302 (2006).
[13] M. Frenklach, D. W. Clary, W. C. Gardiner, and S. E. Stein, Proc. Combust. Inst. **20**, 887 (1985).
[14] M. Frenklach, D. W. Clary, T. Yuan, W. C. Gardiner, and S. E. Stein, Combust. Sci. Technol. **50**, 79 (1986); M. Frenklach, D. W. Clary, W. C. Gardiner, and S. E. Stein, Proc. Combust. Inst. **21**, 1067 (1988); M. Frenklach and J. Warnatz, Combust. Sci. Tech. **51**, 265 (1987).
[15] H. Richter and J. B. Howard, Phys. Chem. Chem. Phys. **4**, 2038 (2002).
[16] H. Richter, W. J. Grieco, and J. B. Howard, Combust. Flame **119**, 1 (1999).
[17] C. Cavallotti, S. Mancarella, R. Rota, and S. Carra, J. Phys. Chem. A **111**, 3959 (2007).
[18] V. V. Kislov and A. M. Mebel, J. Phys. Chem. A **112**, 700 (2008).
[19] V. H. Uc, J. R. Alvarez-Idaboy, A. Galano, I. Garcia-Cruz, and A. Vivier-Bunge, J. Phys. Chem. A **110**, 10155 (2006).
[20] K. Chenoweth, A. C. T. van Duin, and W. A. Goddard III, J. Phys. Chem. A **112**, 1040 (2008).
[21] M. Elstner, D. Porezag, G. Jungnickel, J. Elsner, M. Haugk, T. Frauenheim, S. Suhai, and G. Seifert, Phys. Rev. B **58**, 7260 (1998); G. Seifert, D. Porezag, and T. Frauenheim, Int. J. Quantum Chem. **58**, 185 (1996); D. Porezag, T. Frauenheim, C. Köhler, G. Seifert, and R. Kaschner, Phys. Rev. B **51**, 12947 (1995).
[22] Y. Ohta, Y. Okamoto, S. Irle, and K. Morokuma, ACS Nano **2**, 1437 (2008).
[23] B. M. Bode and M. S. Gordon, J. Mol. Graphics Modell. **16**, 133 (1998).
[24] B. Yang, Y. Li, L. Wei, C. Huang, J. Wang, Z. Tian, R. Yang, L. Sheng, Y. Zhang, and F. Qi, Proc. Combust. Inst. **31**, 555 (2007).
[25] S. Irle, G. Zheng, M. Elstner, and K. Morokuma, Nano Lett. **3**, 1657 (2003).
[26] See supplementary material at http://dx.doi.org/10.1063/1.3447895 for the plot of relative potential, small hydrocarbon species created during simulations, hybridization statistics, snapshots of the structures formed at the end of simulations, number of different rings present in the final structure and its curvature.
[27] M. Frenklach and H. Wang, *Soot Formation in Combustion: Mechanisms and Models* (Springer-Verlag, Heidelberg, 1994).